Ultra-high figure of merit refractive index sensor based on concentric ring and disk resonator

Hui Guo[1] · Zongqiang Chen[1] · Jiwei Qi[1] ·
Meiling Jiang[2] · Jing Chen[1] · Yudong Li[1] · Qian Sun[1]

Abstract   A plasmonic refractive index sensor based on metal–insulator–metal (MIM) waveguide coupled with concentric ring and disk resonator (CRDR) is proposed in this work. The plasmonic refractive index sensor with a sensitivity of 1039 nm/RIU and a high figure of merit (FOM) of 401 in the near-infrared region is numerically investigated using a finite element method (FEM). The physical mechanism of high Q factor of the mode of CRDR can be explained by the coupled mode theory. The structural parameters of the plasmonic sensor are also discussed. The structural parameters can be changed to adjust the sensor properties. Furthermore, the application of proposed plasmonic sensor in bio-sensing is analyzed.

Introduction

Surface plasmon polaritons (SPPs) are charge density waves propagating along the metal–dielectric interface caused by the coupling between photons and electrons on the metal surface [1–3].Their electromagnetic fields decay exponentially in the direction perpendicular to the metal surface. The result is that SPPs can overcome the diffraction limit and have the ability to modulate light in nanoscale [4, 5]. Therefore, many kinds of photonic devices have been investigated, such as filters [6, 7], absorbers [8], all-optical switches [9], and sensors [10–15]. Compared with traditional devices, plasmonic devices have a smaller size to be suitable for integration [4].

Among the plasmonic waveguides, metal–insulator–metal (MIM) waveguides have low transmission loss and are more advantageous of strongly confined the light [16–18]. The sensors based on these structure are basically composed of MIM waveguide coupled with resonators [18–23]. Sensitivity and figure of merit (FOM) are usually used to evaluate the quality of optical sensors. In order to obtain a higher sensitivity and FOM sensor, many photonic devices based on Fano resonance have been proposed [18–23]. Fano resonance is quite sensitive to the change in refractive index; the refractive index sensors can achieve a higher sensitivity [18]. At the same time, Fano resonance has a typically asymmetric and sharp spectral line shape, to achieve a narrower full width at half maximum (FWHM) [20–26]. However, Fano resonance is unstable and easily disturbed by environmental changes. Some works with simple and tunable structure to improve sensing performance have been proposed [27–30].

In this paper, the plasmonic refractive index sensors with a structure composed of MIM waveguide coupled with concentric ring and disk resonator (CRDR) are proposed. In the near-infrared region, a high sensitivity of 1039 nm/RIU with ultra-high FOM of 401 is realized. The influence of the structural parameters of the plasmonic coupling system on sensing properties has also been investigated.

✉ Zongqiang Chen
  chenzongqiang@nankai.edu.cn

  Meiling Jiang
  jiangmeiling@126.com

1   MOE Key Laboratory of Weak Light Nonlinear Photonics, Tianjin Key Laboratory of Photonics Material and Technology, School of Physics, Nankai University, Tianjin 300071, People's Republic of China

2   Guangdong Provincial Key Laboratory of Optical Fiber Sensing and Communications, Institute of Photonics Technology, Jinan University, Guangzhou 510632, China

Structural model and computational method

Figure 1 illustrates the schematic of the 2D metallic microcavity composed of the MIM waveguide and the CRDR. The radius of the cavity is expressed as R, the coupling distance between the MIM waveguide and the CRDR is g, and the gap width between the concentric ring and disk is G. The widths of the MIM waveguide and the ring cavity are fixed at $w = 50$ nm, to ensure that only the fundamental transverse magnetic mode is supported in the MIM waveguide [31].

The white areas and gray areas represent dielectric and metal, respectively. The medium of the dielectric is assumed to be air, and the metal is set to be silver. The dispersion equation of the fundamental TM mode in the MIM structure can be described as follows [32, 33]:

$$\frac{\varepsilon_i p}{\varepsilon_m k} = \frac{1 - e^{kw}}{1 + e^{kw}}$$

$$k = \sqrt{\beta_{spp}^2 - \varepsilon_i k_0^2}$$

$$p = \sqrt{\beta_{spp}^2 - \varepsilon_m k_0^2} \qquad (1)$$

where w is the width of waveguide, β_{spp} is the propagation constant of SPPs, $n_{eff} = \beta_{spp}/k_0$ means effective refractive index of SPPs, $k_0 = 2\pi/\lambda$ refers to wave number, λ is the wavelength of incident light, ε_i and ε_m are relative permittivity of dielectric and metal. The relative permittivity of silver can be characterized by the Drude model [34, 35]:

$$\varepsilon_m = 1 - \frac{\omega_p^2}{\omega(\omega + i\Upsilon)} \qquad (2)$$

here ω_P is the bulk plasma frequency; the bulk plasma frequency ω_p depends on the carrier (holes) density N_h as given in the equation $\omega_p = \left(N_h/\varepsilon_0 m_h\right)^{1/2e}$, where m_h is the hole effective mass, approximated to be $0.8m_0$; m_0 is the electron
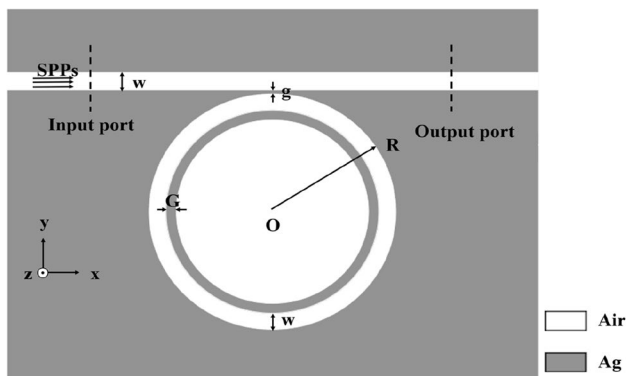
mass. Υ is damping frequency of the electron oscillation, and ω is the incident electromagnetic radiation angular frequency. The parameters of Eq. (2) are $\omega_P = 1.37 \times 10^{16}$ Hz and $\Upsilon = 3.21 \times 10^{13}$ Hz.

For a single ring resonator, the resonating wavelength can be obtained theoretically by the equation [28]:

$$\frac{J_n'(kr_a)}{J_n'(kr_i)} - \frac{N_n'(kr_a)}{N_n'(kr_i)} = 0 \qquad (3)$$

where $k = \omega\left(\varepsilon_0 \varepsilon_r \mu_0\right)^{\frac{1}{2}}$, μ_0 refers to the permeability in the air, $\varepsilon_r = n_{eff}^2/\mu_0$ is the frequency-dependent effective relative permittivity. J_n and J_n' are the first kind Bessel function with the order n and its derivative to the argument (kr); N_n and N_n' are the second kind Bessel function with the order n and its derivative to the argument (kr), respectively.

The resonating wavelength of the disk-shaped nanocavity can be obtained theoretically by the equation [29]:

$$k_i \frac{H_n^{(1)}(k_m r)}{H_n^{(1)}(k_m r)} - k_m \frac{J_n'(k_i r)}{J_n(k_i r)} = 0 \qquad (4)$$

here $k_{i,m} = k\left(\varepsilon_{i,m}\right)^{\frac{1}{2}}$ refers to the wave vectors in the dielectric disk or metal, ε_i and ε_m are the relative permittivity of the dielectric and metal, and k means the wave number. r stands for the radius of the cavity. J_n and J_n' mean the first kind Bessel function with the order n and its derivative; $H_n^{(1)}$ and $H_n^{(1)'}$ refer to the first kind Hankel function with the order n and its derivative, respectively.

In this study, commercial software (COMSOL Multiphysics) of the finite element method (FEM) is used to research the transmission spectra. The two-dimensional (2D) FEM with perfectly matched layer (PML) boundary condition is adopted to simulate this structure and investigate the properties of the refractive index sensing. The transmittance of power is defined to be $T = (S_{21})^2$, where S_{21} is the transmission coefficient from P_{in} to P_{out}[3].

Results and discussion

In this part, the transmission spectra of the MIM waveguide coupled with CRDR are simulated under varying parameters of the structure. Figure 2a shows the simulated transmission spectrum of this structure with $n = 1$, $R = 350$ nm, $g = 10$ nm and $G = 30$ nm. n is the refractive index of the dielectric. Mode 1 and mode 2 can be considered as supermodes in which the inner disk and outer ring can resonate simultaneously [27]. The FWHM of mode 1(λ_1=965 nm) is 17.86 nm, and that of mode 2(λ_2=1038 nm) is 2.59 nm; the Q factors are 54, 401, respectively. Figure 2b and c plots the steady-state magnetic field H_z distributions of the plasmonic

Fig. 1 2D schematic of the plasmonic sensor filled with air

Fig. 2 **a** Transmission spectra of MIM waveguide coupled with CRDR with $n = 1$, $R = 350$ nm, $g = 10$ nm and $G = 30$ nm; steady-state magnetic field H_z distributions of the MIM waveguide coupled with CRDR at wavelengths of (**b**) 964.88 nm; **c** 1038.49 nm
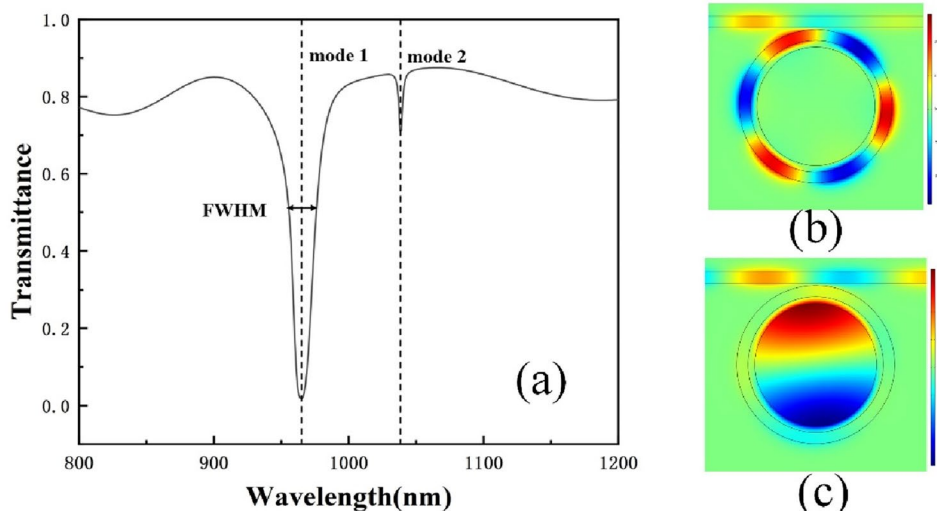
coupling system of mode 1 and mode 2. The ratio of energy confined in the inner disk and the outer ring in mode 1 is 2.78×10^{-3}, and in mode 2 it is 52.1. Energy of CRDR is mainly confined in the inner disk in mode 2, in the out ring in mode 1. The ratio of energy confined in the inner disk and the outer ring is defined as: $R = \int H_{in}^2 dS_{in} / \int H_{out}^2 dS_{out}$, where $\boldsymbol{H_{in}}$ is the magnitude in the inner disk, $\boldsymbol{H_{out}}$ is the magnitude in the outer ring, $\boldsymbol{S_{in}}$ is the area in the inner disk, and $\boldsymbol{S_{out}}$ is the area in the outer ring.

The coupled mode theory [36] is used to explain the principle of high Q factor formation of mode 2 in this paper. Figure 3a shows the transmission spectra of the proposed plasmonic refractive index sensor with inner disk resonator, outer ring resonator or CRDR. Figure 3b plots the steady-state magnetic field H_z distributions of the TM_6 mode of the outer ring resonator. Figure 3c shows the steady-state magnetic field H_z distributions of the TM_2 mode of the inner

disk resonator. The transmission spectrum of the CRDR is almost the superposition of the outer ring transmission spectra and inner disk transmission spectra. In order to meet the angular momentum matching condition, the strong coupling is more prone to take place between the same order modes between the inner disk and outer ring. Figure 4 presents the diagram of mode coupling between the TM_2 modes of the inner disk and outer ring of the CRDR. Mode 2 is corresponded to quasi-in-phase CRDR mode. Owing to the asymmetry between the inside and outside of the CRDR structure, the resonance frequency difference between different order modes of inner disk and outer ring becomes smaller as shown in our results. Thus, TM_6 mode of the outer ring resonator has an impact on the quasi-in-phase CRDR mode. The final simulation result shows that Quasi-in-phase mode 2 has a narrow resonance dip and exhibits a little red shift. This phenomenon can be explained by the fact that the

Fig. 3 **a** Transmission spectra of the proposed plasmonic refractive index sensor with inner disk resonator, outer ring resonator or CRDR. **b** Steady-state magnetic field H_z distributions of TM_6 mode of the outer ring resonator at wavelengths of 948.19 nm. **c** Steady-state magnetic field H_z distributions of TM_2 mode of the inner disk resonator at wavelengths of 1034.96 nm
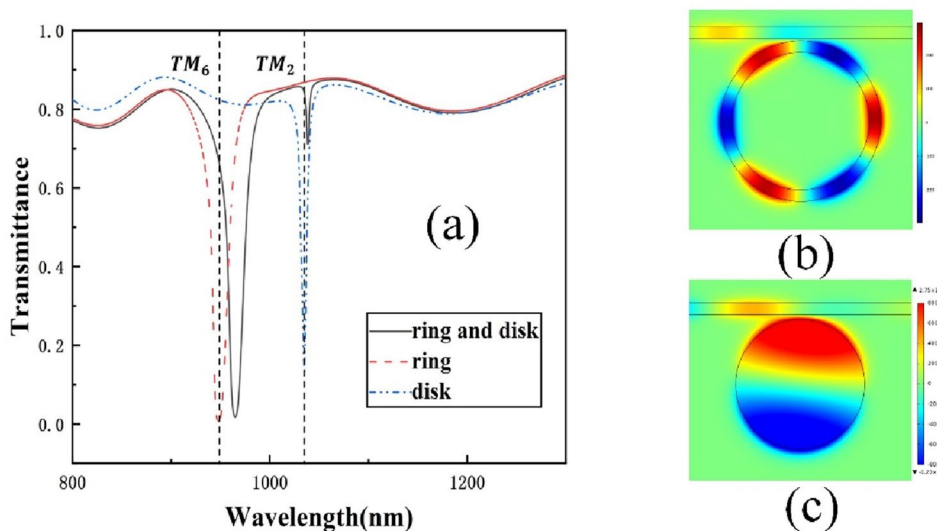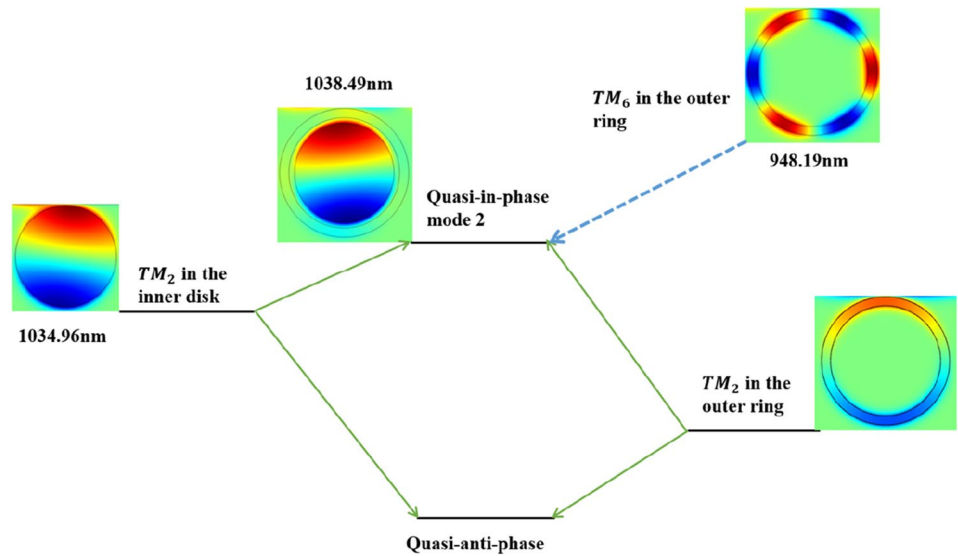
Fig. 4 Schematic of the mode coupling between the TM_2 modes of the inner disk and outer ring of the CRDR

quasi-in-phase mode is closer to the inner disk mode and the energy of electromagnetic wave mainly confines in the inner disk. Because of the outer ring, the energy in the inner disk is more difficult to loss and is beneficial for energy storage. Therefore, the resonance dip induced by the quasi-in-phase mode 2 is very narrow which leads to ultra-small FWHM and ultra-high Q factor.

To research the effect of the refractive index of dielectric on the structure, we use different media to fill the structure; the transmission spectra are presented in Fig. 5a. The n is increased from 1 to 1.08 by the step 0.02. A red shift the transmission spectrum can be observed with an increase in n. The increase in the resonance wavelength is in line with the theoretical calculation result of formula 4 [29]. In this study, we use S and FOM to measure the sensing performance. They are defined as follows [37, 38]:

$$S = \frac{\Delta\lambda}{\Delta n} \tag{5}$$

$$FOM = \frac{S}{FWHM} \tag{6}$$

As shown in Fig. 5b, the sensitivity can be calculated by linear fitting. For mode 1, S is 971 nm/RIU; FOM is 54. For mode 2, S is 1039 nm/RIU; FOM is 401. Mode 2 is further investigated then in view of its excellent sensing performance in the near-infrared region.

To investigate the influences of different cavities on the transmission spectra and sensor performance, R is varied from 330 to 370 nm at intervals of 10 nm with $n=1$, $g=10$ nm and $G=30$ nm. Figure 6a plots the transmission spectra of the structure of $R=330$, 340, 350, 360 and

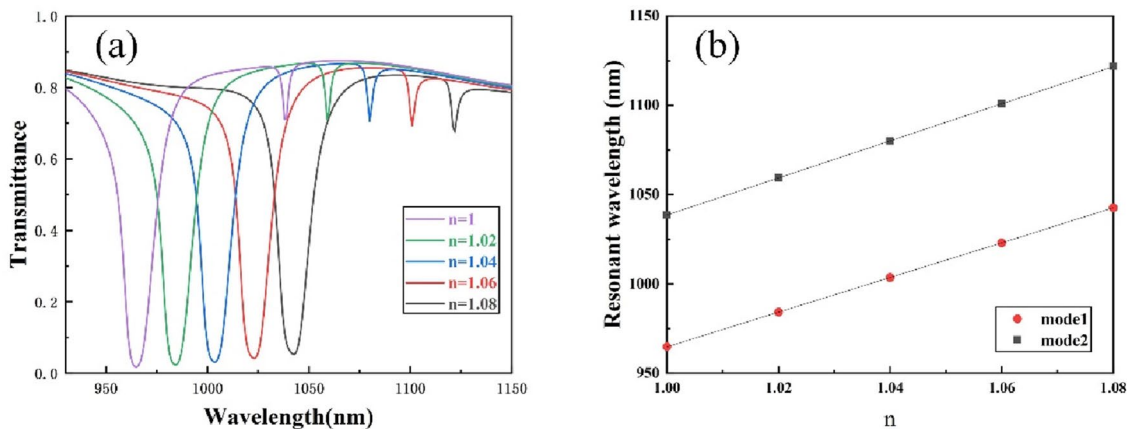**Fig. 5 a** Transmission spectra for the MIM waveguide coupled with CRDR with changing n while $R=350$ nm g $=10$ nm and $G=30$ nm; **b** fitting curve between refractive index and resonant wavelength
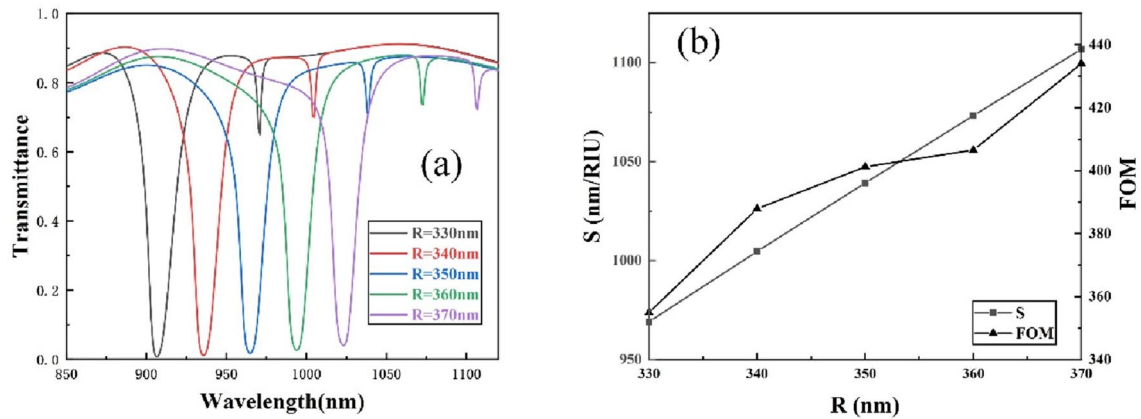
Fig. 6 **a** Transmission spectra of the MIM waveguide coupled with CRDR with changing radius of the cavity; **b** sensitivity and figure of merit of the sensor structure for different values of R

370 nm. With the increasing radius of the cavity, the transmission spectrum exhibits a red shift as shown in Fig. 6a. The increase in the resonance wavelength of mode 1 and mode 2 also accords with the theoretical calculation results of formulas 3 and 4 [29, 32]. As the radius increases, the shape of the transmission spectrum remains nearly constant. Figure 6b shows S and FOM of the plasmonic sensor for different values of *R*. Obviously, S and FOM of the plasmonic sensor can be improved by increasing the size of CRDR. When *R* = 370 nm, the sensor gets the maximum S and FOM, S = 1107 nm/RIU, FOM = 434.

The coupling distance between the MIM waveguide and the CRDR is changed to study its influences on the transmission spectra and sensor performance. The coupling distance *g* is increased from 6 nm to 14 in steps of 2 nm while the other parameters are fixed at *n* = 1, *R* = 350 nm and *G* = 30 nm. The transmission spectra of different

coupling distance are shown in Fig. 7a. The simulation results show that for mode 2, when g increases from 6 to 14 nm, the transmittance of the resonance dip is significantly increased. This outcome can be explained the increase in coupling distance allows less energy to enter the CRDR, resulting in a higher transmittance. At the same time, the transmission spectrum also has a slight blue shift, which is consistent with the results in reference [29]. Figure 7b shows S and FOM of the plasmonic sensor for different values of *g*. The sensitivity of the plasmonic sensor is almost unchanged as the *g* increases, but the value of FOM can be significantly increased because of the narrower resonance dip. Maximum sensitivity of 1040 can be reached when *g* = 6 nm/RIU, and the value of the maximum FOM is 433 when *g* = 14 nm.

For the investigation of the effect of the different gap width between the concentric ring and disk on the transmission spectra and sensor performance, *G* is increased
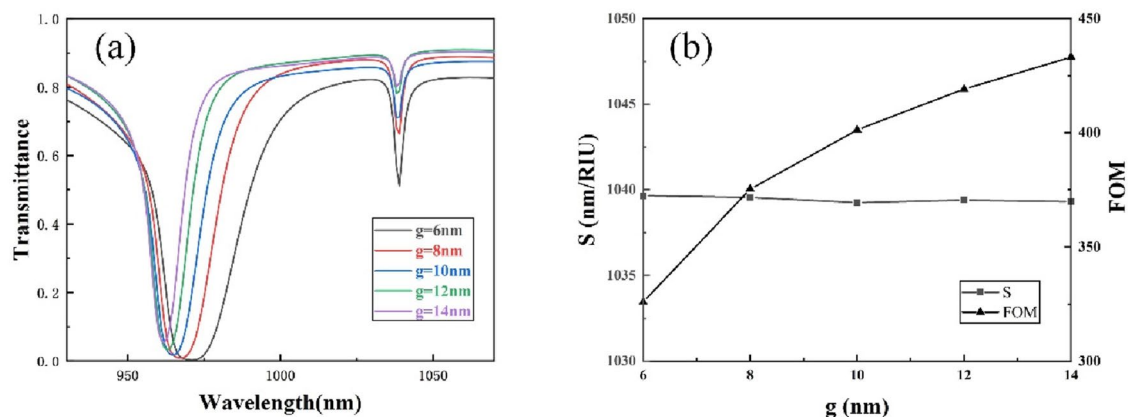

Fig. 7 **a** Transmission spectra of the MIM waveguide coupled with CRDR with changing coupling distance between the MIM waveguide and the CRDR; **b** sensitivity and figure of merit of the sensor structure for different values of g

from 20 to 40 nm at 5-nm intervals, with $n=1$, $R=350$ nm and $g=10$ nm. The transmission spectra of the structure with the different gap width of G are shown in Fig. 8a. With the increasing gap width, blue shifts in the transmission spectrum can be observed. The blue shift of the mode 2 resonance wavelength is caused by the decrease in the radius of the inner circular cavity. And for the mode 2, the transmittance of the dip is significantly increased as G increasing. This phenomenon can be explained that the increase in the gap width allows less energy to enter the inner circular cavity, which leads a higher transmittance. Figure 8b presents S and FOM of the plasmonic sensor with increasing G. Although the sensitivity shows a decrease as G increases, the FOM still improves because of the narrower resonance dip. There is a compromise between high sensitivity and high FOM. The maximum sensitivity of the structure when $G=20$ nm is 1085 nm/RIU, and the maximum FOM is 471 when $G=40$ nm. With the increasing gap width, blue shifts in the transmission spectrum can be observed. And for the mode 2, the transmittance of the dip is significantly increased as G increasing. This phenomenon can be explained that the increase in the gap width allows less energy to enter the inner circular cavity, which leads a higher transmittance. When G is nearly to 0, the mode 1 with energy concentrated in the outer ring disappears, and the transmission spectra become the transmission spectra of the disk resonator.

To discuss the application of the proposed plasmonic sensor in bio-sensing, another simulation is performed near the refractive index of 1.33. The n is increased from 1.30 to 1.38 with the step 0.02 while the other parameters are fixed at $R=350$ nm $g=10$ nm and $G=30$ nm; the transmission spectra are presented in Fig. 9. It can be seen that the sensitivity and FOM of the plasmonic sensor near the refractive index of water can still reach 1035 nm/RIU and 234, showing excellent sensing performance. Table 1 presents
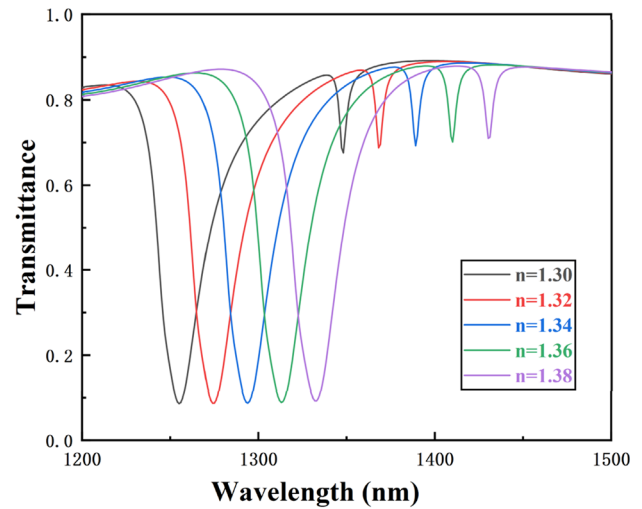

Fig. 9 Transmission spectra for the MIM waveguide coupled with CRDR with changing n while R = 350 nm g = 10 nm and G = 30 nm

the comparison of the S and the FOM in our work and in some other recent works; our work shows ultra-high FOM.

Conclusions

In this work, a plasmonic refractive index sensor based on MIM waveguides coupled with CRDR is proposed. Our proposed plasmonic structure presents ultra-high Q factor in the quasi-in-phase mode. With the increase in the radius of the cavity, both sensitivity and the value of FOM show an obvious increase. As the coupling distance increases, the sensitivity of the plasmonic sensor remains nearly constant, but the value of FOM can be significantly improved. With an increase in the gap width between the concentric ring and disk, the FOM of the plasmonic sensor shows an increase,
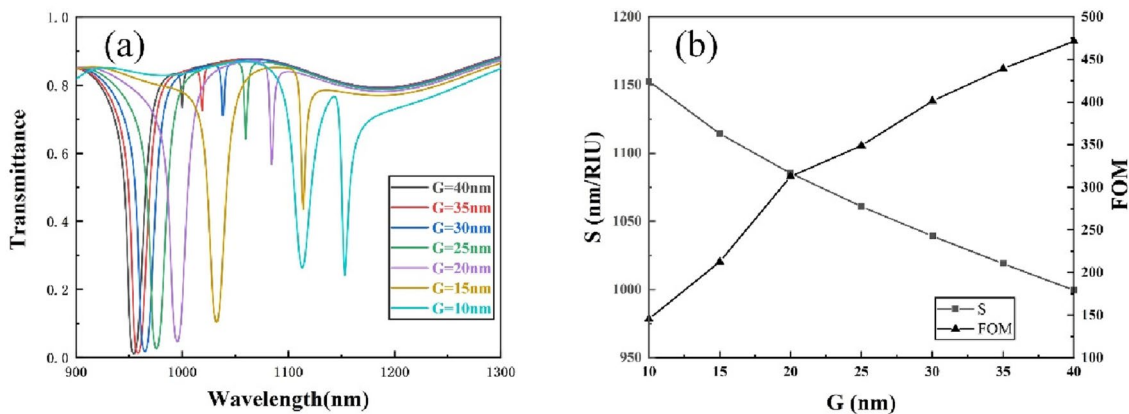

Fig. 8 **a** Transmission spectra of the MIM waveguide coupled with CRDR with changing gap width between the concentric ring and disk; **b** sensitivity and figure of merit of the sensor structure for different values of G

Table 1 Comparison of the S and the FOM in our work and in some other recent works

References	Year	S(nm/RIU)	FOM
[17]	2018	1060	203.8
[27]	2020	1270	58
[39]	2021	550	282.5
[40]	2018	1100	224
[41]	2021	1025	125
[42]	2020	2380 for mode 2 and 959 for mode 1	–
This work ($n=1$)	–	1039	401
This work ($n=1.33$)	–	1035	234

but sensitivity decreases. High sensitivity with ultra-high FOM can be reached in the near-infrared region. The max refractive index sensitivity of the sensor is 1107 nm/RIU, and the FOM can reach 471. In addition, this plasmonic structure has great potential in bio-sensing and can be easily integrated with other photonic devices.

References

1. W.L. Barnes, A. Dereux, T.W. Ebbesen, Surface plasmon subwavelength optics. Nature **424**, 824–830 (2003). https://doi.org/10.1038/nature01937
2. A.V. Zayats, I.I. Smolyaninov, A.A. Maradudin, Nano-optics of surface plasmon polaritons. Phys. Rep. Rev. Sect. Phys. Lett. **408**, 131–314 (2005). https://doi.org/10.1016/j.physrep.2004.11.001
3. X.F. Zhao, Z.D. Zhang, S.B. Yan, Tunable fano resonance in asymmetric MIM waveguide structure. Sensors. **17**, 1–8 (2017). https://doi.org/10.3390/s17071494
4. H. Lu, X.M. Liu, D. Mao, G.X. Wang, Plasmonic nanosensor based on Fano resonance in waveguide-coupled resonators. Opt. Lett. **37**, 3780–3782 (2012). https://doi.org/10.1364/ol.37.003780
5. Y. Tang, Z.D. Zhang, R.B. Wang, Z.Y. Hai, C.Y. Xue, W.D. Zhang, S.B. Yan, Refractive index sensor based on fano resonances in metal-insulator-metal waveguides coupled with resonators. Sensors. **17**, 1–8 (2017). https://doi.org/10.3390/s17040784
6. X.S. Lin, X.G. Huang, Tooth-shaped plasmonic waveguide filters with nanometeric sizes. Opt. Lett. **33**, 2874–2876 (2008). https://doi.org/10.1364/ol.33.002874
7. Y.P. Qi, P.Y. Zhou, T. Zhang, X.W. Zhang, Y. Wang, C.Q. Liu, Y.L. Bai, X.X. Wang, Theoretical study of a multichannel plasmonic waveguide notch filter with double-sided nanodisk and two slot cavities. Res. Phys. **14**, 102506 (2019). https://doi.org/10.1016/j.rinp.2019.102506
8. D. Wu, C. Liu, Y.M. Liu, L. Yu, Z.Y. Yu, L. Chen, R. Ma, H. Ye, Numerical study of an ultra-broadband near-perfect solar absorber in the visible and near-infrared region. Opt. Lett. **42**, 450–453 (2017). https://doi.org/10.1364/ol.42.000450
9. H. Lu, X.M. Liu, L.R. Wang, Y.K. Gong, D. Mao, Ultrafast all-optical switching in nanoplasmonic waveguide with Kerr nonlinear resonator. Opt. Express **19**, 2910–2915 (2011). https://doi.org/10.1364/oe.19.002910
10. C.T.C. Chao, Y.F.C. Chau, H.J. Huang, N. Kumara, M.R.R. Kooh, C.M. Lim, H.P. Chiang, Highly sensitive and tunable plasmonic sensor based on a nanoring resonator with silver nanorods. Nanomaterials **10**, 1–14 (2020). https://doi.org/10.3390/nano10071399
11. M.S. Islam, J. Sultana, A.A. Rifat, R. Ahmed, A. Dinovitser, B.W.H. Ng, H. Ebendorff-Heidepriem, D. Abbott, Dual-polarized highly sensitive plasmonic sensor in the visible to near-IR spectrum. Opt. Express **26**, 30347–30361 (2018). https://doi.org/10.1364/oe.26.030347
12. M.J. Al-mamod, R. Hyder, M.Z. Islam, Numerical studies on a plasmonic temperature nanosensor based on a metal-insulator-metal ring resonator structure for optical integrated circuit applications. Photon. Nanostruct. Fundam. Appl. **25**, 52–57 (2017). https://doi.org/10.1016/j.photonics.2017.05.001
13. S.N. Khonina, N.L. Kazanskiy, M.A. Butt, Evanescent field ratio enhancement of a modified ridge waveguide structure for methane gas sensing application. IEEE Sens. J. **20**, 8469–8476 (2020). https://doi.org/10.1109/jsen.2020.2985840
14. G.G. Qiu, Z.B. Gai, Y.L. Tao, J. Schmitt, G.A. Kullak-Ublick, J. Wang, Dual-functional plasmonic photothermal biosensors for highly accurate severe acute respiratory syndrome coronavirus 2 detection. ACS Nano **14**, 5268–5277 (2020). https://doi.org/10.1021/acsnano.0c02439
15. F. Lotfi, N. Sang-Nourpour, R. Kheradmand, High-sensitive plasmonic sensor based on Mach-Zehnder interferometer. Opt. Laser Technol. **137**, 106809 (2021). https://doi.org/10.1016/j.optlastec.2020.106809
16. Z.D. Zhang, H.Y. Wang, Y.N. Zhao, D. Lu, Z.Y. Zhang, Transmission properties of the one-end-sealed metal-insulator-metal waveguide. Optik **124**, 177–179 (2013). https://doi.org/10.1016/j.ijleo.2011.11.066
17. Z.J. Zhang, J.B. Yang, X. He, J.J. Zhang, J. Huang, D.B. Chen, Y.X. Han, Plasmonic refractive index sensor with high figure of merit based on concentric-rings resonator. Sensors. **18**, 1–14 (2018). https://doi.org/10.3390/s18010116
18. S.B. Yan, L. Luo, C.Y. Xue, Z.D. Zhang, A refractive index sensor based on a metal-insulator-metal waveguide-coupled ring resonator. Sensors. **15**, 29183–29191 (2015). https://doi.org/10.3390/s151129183
19. Z.D. Zhang, L. Luo, C.Y. Xue, W.D. Zhang, S.B. Yan, Fano resonance based on metal-insulator-metal waveguide-coupled double rectangular cavities for plasmonic nanosensors. Sensors. **16**, 1–10 (2016). https://doi.org/10.3390/s16050642
20. J.J. Chen, Z. Li, Y.J. Zou, Z.L. Deng, J.H. Xiao, Q.H. Gong, Coupled-resonator-induced fano resonances for plasmonic sensing with ultra-high figure of merits. Plasmonics **8**, 1627–1631 (2013). https://doi.org/10.1007/s11468-013-9580-4
21. M. Rahmatiyar, M. Afsahi, M. Danaie, Design of a refractive index plasmonic sensor based on a ring resonator coupled to a MIM waveguide containing tapered defects. Plasmonics **15**, 2169–2176 (2020). https://doi.org/10.1007/s11468-020-01238-z
22. A. Hocini, H. Ben Salah, D. Khedrouche, N. Melouki, A high-sensitive sensor and band-stop filter based on intersected double ring resonators in metal-insulator-metal structure. Opt. Quant. Electr. **52**, 336 (2020). https://doi.org/10.1007/s11082-020-02446-x
23. R. El Haffar, A. Farkhsi, O. Mahboub, Optical properties of MIM plasmonic waveguide with an elliptical cavity resonator. Appl.

Phys. A-Mater. Sci. Process. **126**(486), 1–10 (2020). https://doi.org/10.1007/s00339-020-03660-w

24. A.E. Miroshnichenko, S. Flach, Y.S. Kivshar, Fano resonances in nanoscale structures. Rev. Mod. Phys. **82**, 2257–2298 (2010). https://doi.org/10.1103/RevModPhys.82.2257

25. W. Su, Y.M. Ding, Y.L. Luo, Y. Liu, A high figure of merit refractive index sensor based on Fano resonance in all-dielectric metasurface. Res. Phys. **16**, 102833 (2020). https://doi.org/10.1016/j.rinp.2019.102833

26. S. Karmakar, D. Kumar, R.K. Varshney, D.R. Chowdhury, Strong terahertz matter interaction induced ultrasensitive sensing in Fano cavity based stacked metamaterials. J. Phys. D-Appl. Phys. **53**, 415101 (2020). https://doi.org/10.1088/1361-6463/ab94e3

27. S. Asgari, S. Pooretemad, N. Granpayeh, Plasmonic refractive index sensor based on a double concentric square ring resonator and stubs. Photon. Nanostruct. Fundam. Appl. **42**, 100857 (2020). https://doi.org/10.1016/j.photonics.2020.100857

28. T.S. Wu, Y.M. Liu, Z.Y. Yu, Y.W. Peng, C.G. Shu, H. Ye, The sensing characteristics of plasmonic waveguide with a ring resonator. Opt. Express **22**, 7669–7677 (2014). https://doi.org/10.1364/oe.22.007669

29. H. Lu, X.M. Liu, D. Mao, L.R. Wang, Y.K. Gong, Tunable bandpass plasmonic waveguide filters with nanodisk resonators. Opt. Express **18**, 17922–17927 (2010). https://doi.org/10.1364/oe.18.017922

30. L. Chen, Y.M. Liu, Z.Y. Yu, D. Wu, R. Ma, Y. Zhang, H. Ye, Numerical analysis of a near-infrared plasmonic refractive index sensor with high figure of merit based on a fillet cavity. Opt. Express **24**, 9975–9983 (2016). https://doi.org/10.1364/oe.24.009975

31. R.D. Kekatpure, A.C. Hryciw, E.S. Barnard, M.L. Brongersma, Solving dielectric and plasmonic waveguide dispersion relations on a pocket calculator. Opt. Express **17**, 24112–24129 (2009). https://doi.org/10.1364/oe.17.024112

32. T.B. Wang, X.W. Wen, C.P. Yin, H.Z. Wang, The transmission characteristics of surface plasmon polaritons in ring resonator. Opt. Express **17**, 24096–24101 (2009). https://doi.org/10.1364/oe.17.024096

33. I.P. Kaminow, W.L. Mammel, H.P. Weber, Metal-clad optical waveguides: analytical and experimental study. Appl. Opt. **13**, 396–405 (1974). https://doi.org/10.1364/AO.13.000396

34. P.B. Johnson, R.W. Christy, Optical constants of the noble metals. Phys. Rev. B **6**, 4370–4379 (1972). https://doi.org/10.1103/PhysRevB.6.4370

35. M.L. Jiang, J.W. Qi, M.S. Zhang, Q. Sun, J. Chen, Z.Q. Chen, X.Y. Yu, Y.D. Li, J.G. Tian, Ultra-high quality factor metallic micro-cavity based on concentric double metal-insulator-metal rings. Sci. Rep. **7**, 15663 (2017). https://doi.org/10.1038/s41598-017-15906-4

36. L. Zhang, M.P. Song, T. Wu, L.G. Zou, R.G. Beausoleil, A.E. Willner, Embedded ring resonators for microphotonic applications. Opt. Lett. **33**, 1978–1980 (2008). https://doi.org/10.1364/ol.33.001978

37. L.J. Sherry, S.H. Chang, G.C. Schatz, R.P. Van Duyne, B.J. Wiley, Y.N. Xia, Localized surface plasmon resonance spectroscopy of single silver nanocubes. Nano Lett. **5**, 2034–2038 (2005). https://doi.org/10.1021/nl0515753

38. R. Ameling, L. Langguth, M. Hentschel, M. Mesch, P.V. Braun, H. Giessen, Cavity-enhanced localized plasmon resonance sensing. Appl. Phys. Lett. **97**, 253166 (2010). https://doi.org/10.1063/1.3530795

39. S. Khani, M. Hayati, An ultra-high sensitive plasmonic refractive index sensor using an elliptical resonator and MIM waveguide. Superlatt. Microstruct. (2021). https://doi.org/10.1016/j.spmi.2021.106970

40. R. Zafar, S. Nawaz, G. Singh, A. D'Alessandro, M. Salim, Plasmonics-based refractive index sensor for detection of hemoglobin concentration. IEEE Sens. J. **18**, 4372–4377 (2018). https://doi.org/10.1109/jsen.2018.2826040

41. H. Mathuriya, R. Zafar, G. Singh, Plasmonic grating-based refractive index sensor with high sensitivity. IETE J. Res. (2021). https://doi.org/10.1080/03772063.2021.1925600

42. S. Achi, A. Hocini, H. Ben Salah, A. Harhouz, refractive index sensor MIM based waveguide coupled with a slotted side resonator. Prog. Electromag. Res. M **96**, 147–156 (2020). https://doi.org/10.2528/PIERM20061803

Publisher's Note Springer Nature remains neutral with regard to jurisdictional claims in published maps and institutional affiliations.